Supplementary Information

Nanoscale control of disorder-to-order layer-stacking boosts multiferroic responses in an Aurivillius-type layered oxide

Shujie Sun[1,2*], Yuan Li[1], Xiaofeng Yin[1], Changhui Liu[3], Xiaoning Li[4], Ruixia Ti[5]
Liang Fang[1], Tianfu Zhang[1], Ranran Peng[2] and Yalin Lu[2]

[1] Collaborative Innovation Center of Henan Province for Energy-Saving Building Materials, Xinyang Normal University, Xinyang, 464000, China.

[2] Department of Materials Science and Engineering, University of Science and Technology of China, Hefei, 230026, China.

[3] Department of Chemical and Biomolecular Engineering, National university of Singapore, Singapore, 117585, Singapore.

[4] Institute for Superconducting and Electronic Materials, University of Wollongong, Wollongong 2500, Australia.

[5] College of Physics and Electronic Engineering, Xinxiang University, Xinxiang, 453003, China.

** Corresponding Author: sjsun@xynu.edu.cn.*

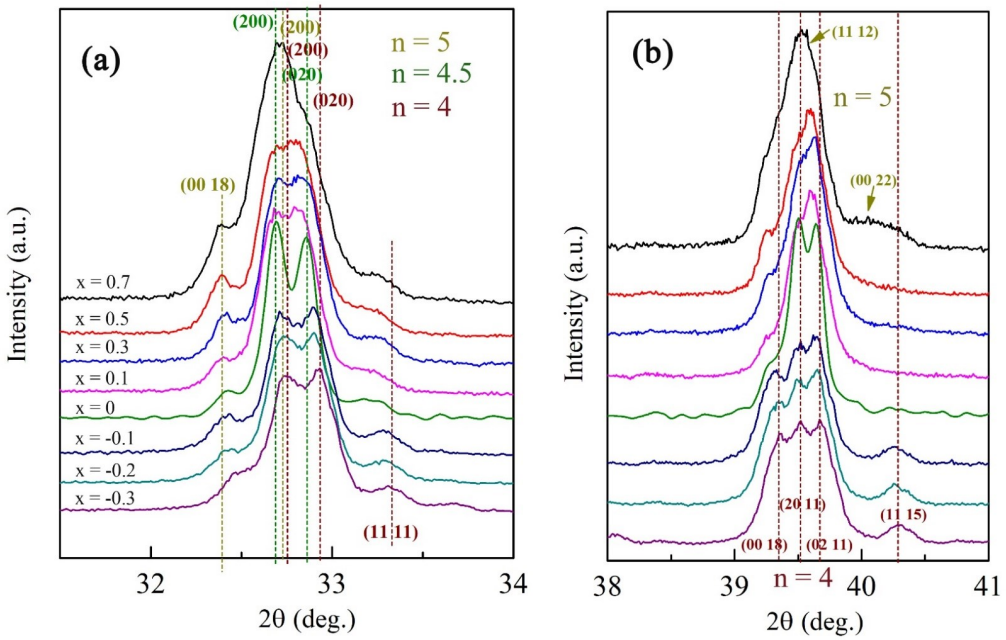

Figure S1. *Magnified XRD patterns of the sintered $Bi_{11}Fe_{3+x}Ti_{6-x}O_{33}$ ceramic powders in the 2θ range of (a) 32-34° and (b) 39-41°.*

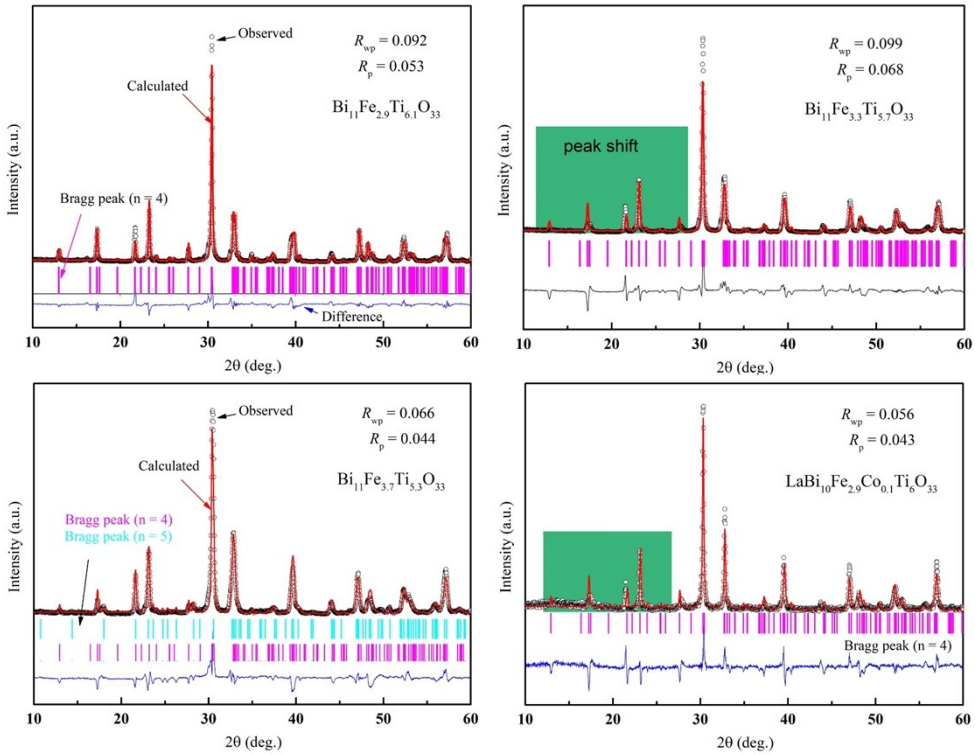

Figure S2 *Rietveld refinements for the powder XRD patterns of the sintered $Bi_{11}Fe_{2.9}Ti_{6.1}O_{33}$ (x = -0.1), $Bi_{11}Fe_{3.3}Ti_{5.7}O_{33}$ (x = 0.3), $Bi_{11}Fe_{3.7}Ti_{5.3}O_{33}$ (x = 0.7) and $LaBi_{10}Fe_{2.9}Co_{0.1}Ti_6O_{33}$ (y = 0.1; z = 1.0) ceramics. These XRD patterns were refined in the orthorhombic lattice using GSAS software. Circles indicate the experimental data and calculated data are the continuous red line overlapping them. The blue curve shows the difference between the experimental and calculated*

patterns. The vertical bars indicate the expected reflection positions.

The lattice parameters and space groups turn out to be a = 5.46 Å, b = 5.43 Å, c = 41.18 Å for x = -0.1 ($A2_1am$-$Bi_5FeTi_3O_{15}$), a = 5.45 Å, b = 5.46 Å, c = 40.97 Å for x = 0.3 ($A2_1am$-$Bi_5FeTi_3O_{15}$ as an example), a = 5.45 Å, b = 5.43 Å, c = 40.99 Å, and a = 5.48 Å, b = 5.45 Å, c = 49.2 Å for x = 0.7 ($A2_1am$- $Bi_5FeTi_3O_{15}$ and F2mm-$Bi_6Fe_2Ti_3O_{15}$), and a = 5.464 Å, b = 5.459 Å, c = 41.07 Å for $LaBi_{10}Fe_{2.9}Co_{0.1}Ti_6O_{33}$ ($A2_1am$- $Bi_5FeTi_3O_{15}$ as an example). In addition, the lattice parameters and space groups turn out to be a = 5.52 Å, b = 5.59 Å, c = 46.4 Å for x = 0.3, and a = 5.45 Å, b = 5.46 Å, c = 45.8 Å for $LaBi_{10}Fe_{2.9}Co_{0.1}Ti_6O_{33}$, when the XRD patterns were fined by the standard B2mm-$Bi_{11}Fe_3Ti_6O_{33}$ using the JADE software.

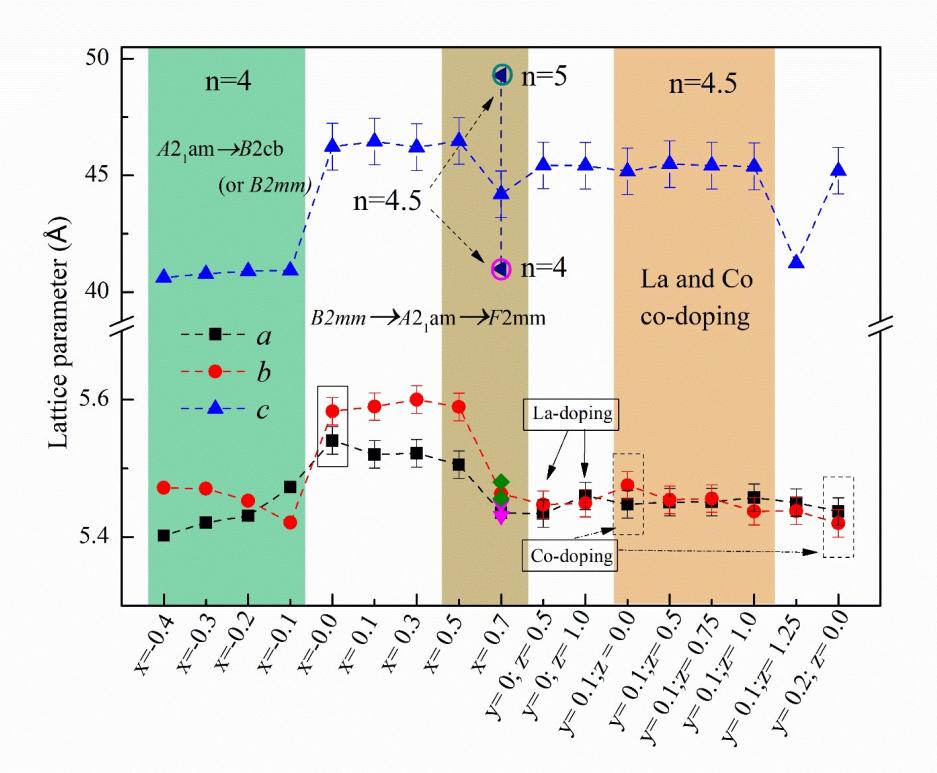

Figure. S3 *Lattice constants of the $Bi_{11}Fe_{3+x}Ti_{6-x}O_{33}$ (x) and $La_zBi_{11-z}Fe_{3-y}Co_yTi_6O_{33}$ (y, z) refined by the Rietveld method. These XRD patterns were refined in the orthorhombic lattice using GSAS software and JADE-5 software. For the mixed-layer structure, there are no suitable crystal structures (CIF format files). The calculated results are from the proportional average values by using $Bi_{11}Fe_3Ti_6O_{33}$.cif and $Bi_5FeTi_3O_{15}$.cif. The width of the error bar is 1 Å for c and 0.02 Å for a and b.*

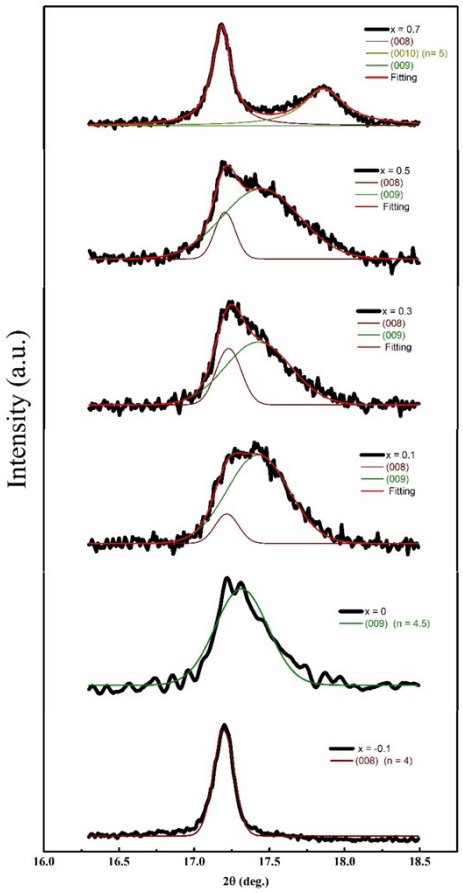

Figure S4. *The fitted peak of the sintered $Bi_{11}Fe_{3+x}Ti_{6-x}O_{33}$ ceramic powders at 16.3-18.5° and the curve was decomposed into Lorentz components.*

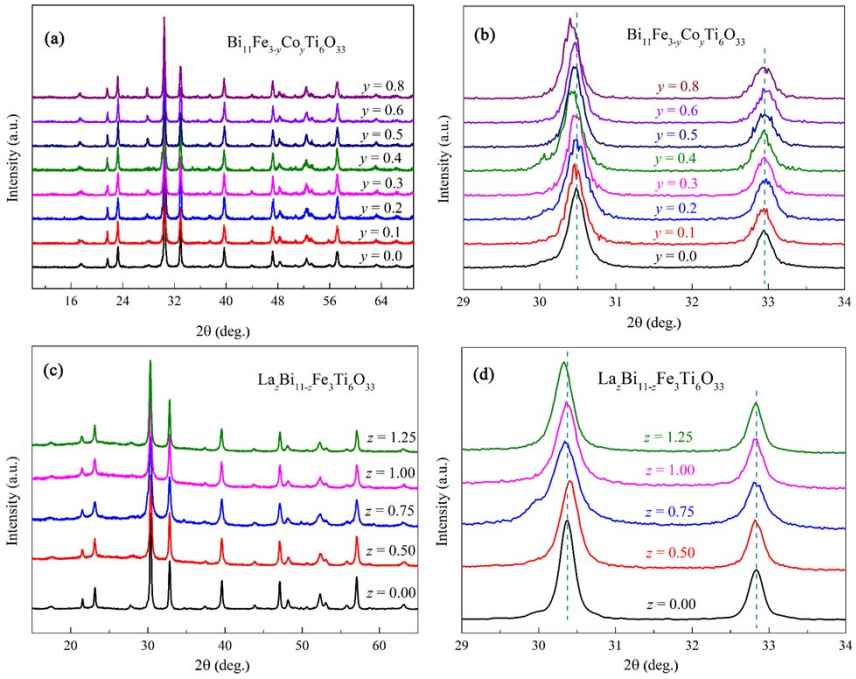

Figure S5. *XRD patterns of the calcined (a) $Bi_{11}Fe_{3-y}Co_yTi_6O_{33}$ and (c) $La_zBi_{11-z}Fe_3Ti_6O_{33}$ powders at 700℃, and (b and c) their magnified sections in the 2θ range of (b) 29°-34°.*

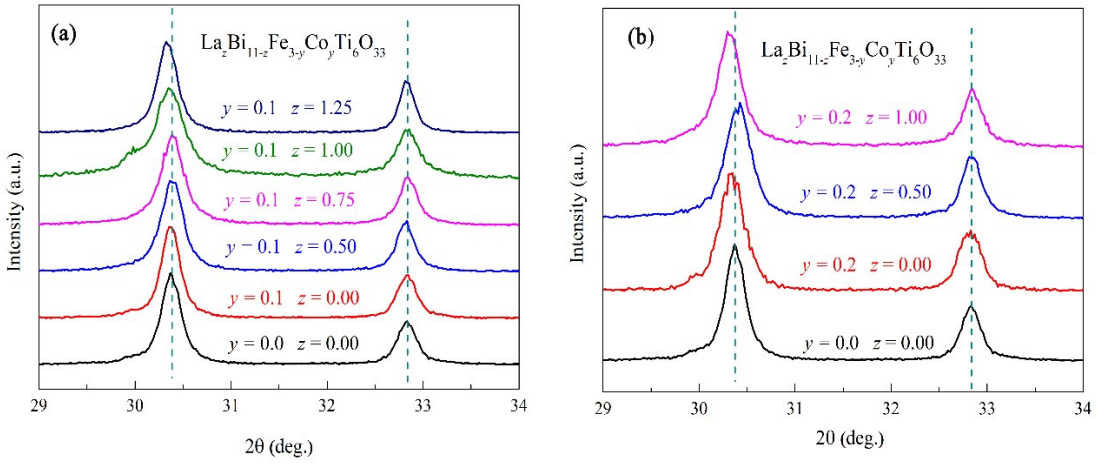

Figure S6. *Magnified XRD patterns of the calcined $La_zBi_{11-z}Fe_{3-y}Co_yTi_6O_{33}$ powders at 700℃/2h in the 2θ range of 29°-34°: (a) y =0.1 and (b) y = 0.2.*

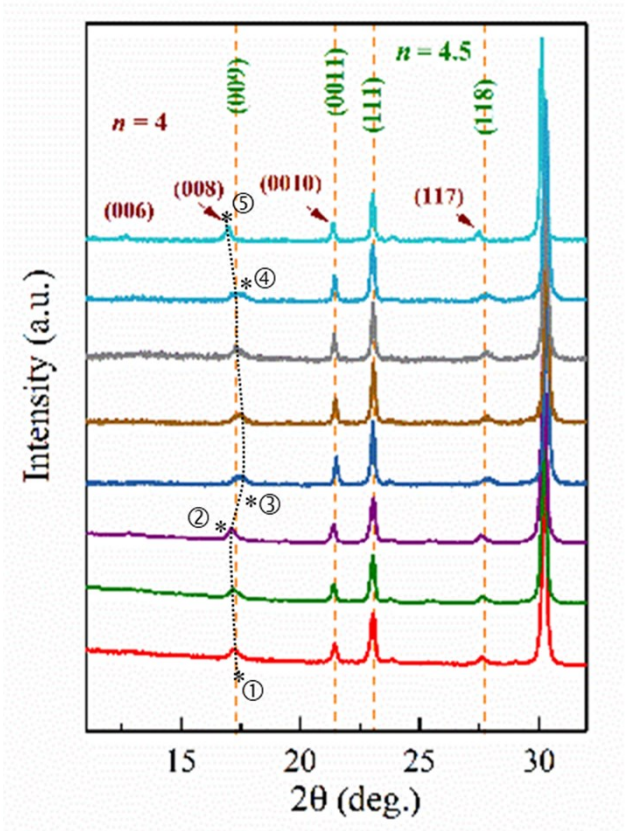

Figure S7. *Magnified XRD pattern of the sintered $La_zBi_{11-z}Fe_{3-y}Co_yTi_6O_{33}$ powders at 950℃ in the 2θ range of 12°-33° (data from Figure 2d).*

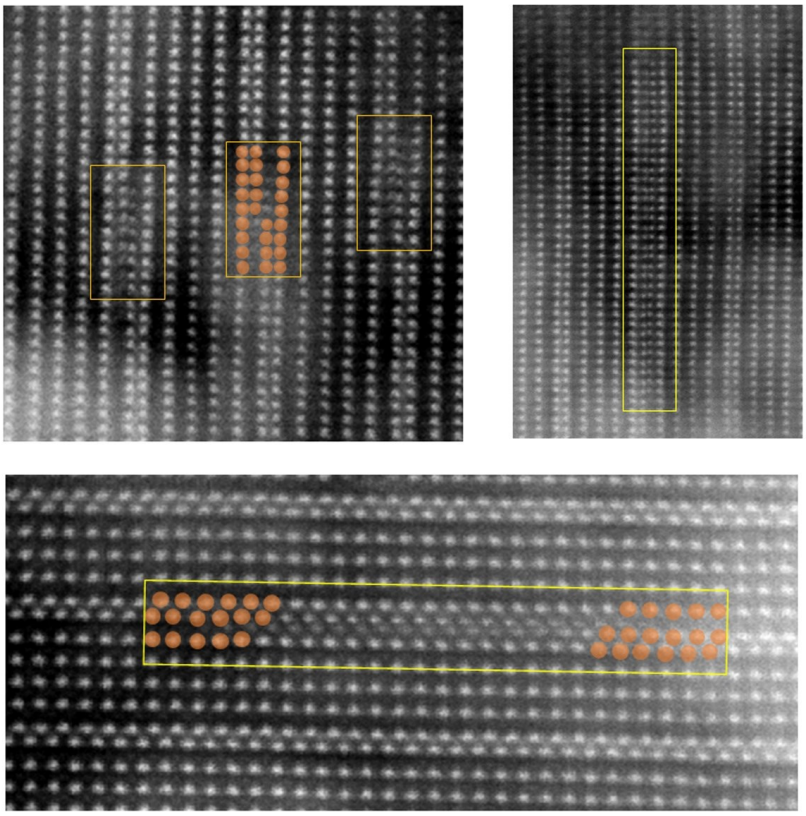

Figure S8. *Representative atomic resolution images in a region of the crystallite displaying OPBs-related defects from the Figures 3a and 3b, to highlight the characters of the defects.*

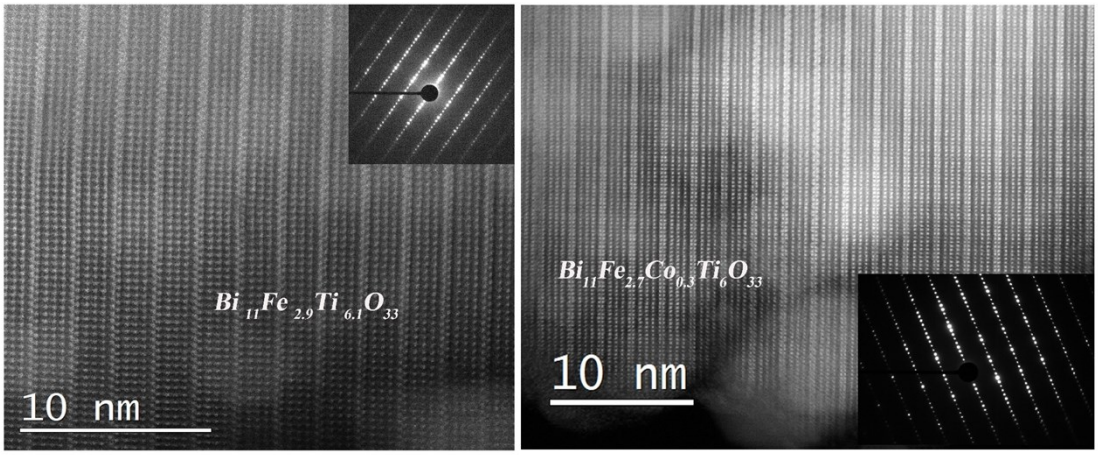

Figure S9. *STEM-HAADF images and the selected area electron diffraction (SAED) patterns of* $Bi_{11}Fe_{2.9}Ti_{6.1}O_{33}$ *and* $Bi_{11}Fe_{2.7}Co_{0.3}Ti_6O_{33}$.

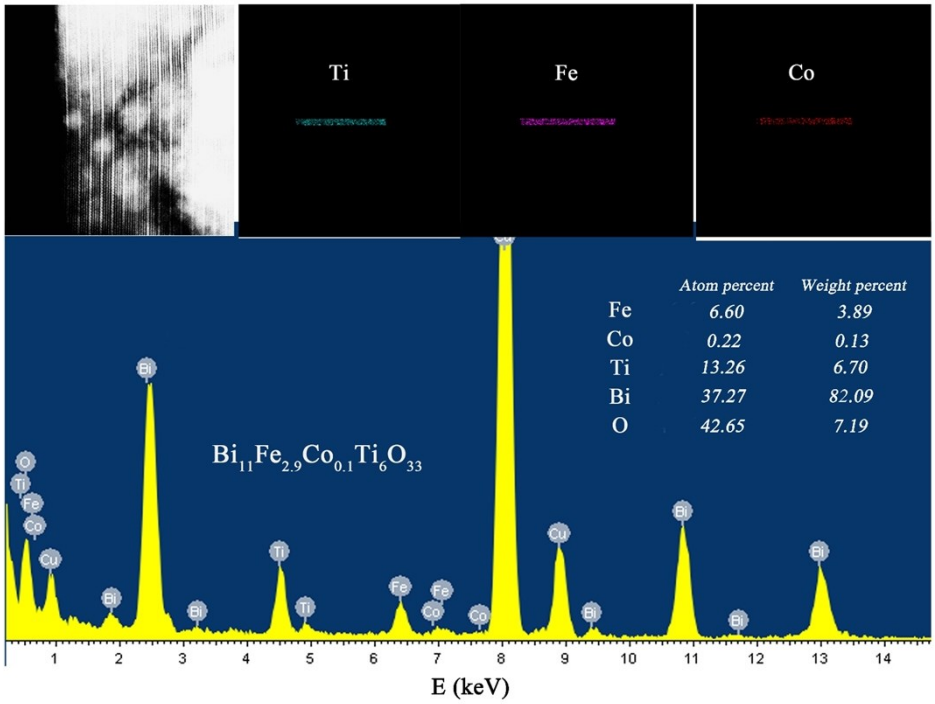

Figure S10 *STEM-EDX spectrum and element mapping images of $Bi_{11}Fe_{2.9}Co_{0.1}Ti_6O_{33}$. The microstructure of the sample is composed of Bi, Ti, Fe, Co and O, and the metal elements distribute homogeneously in the selected area. The atomic ratio of Fe, Co and Ti is approximately 30:1:60.3, in good agreement with the formula of the sample (29:1:60).*

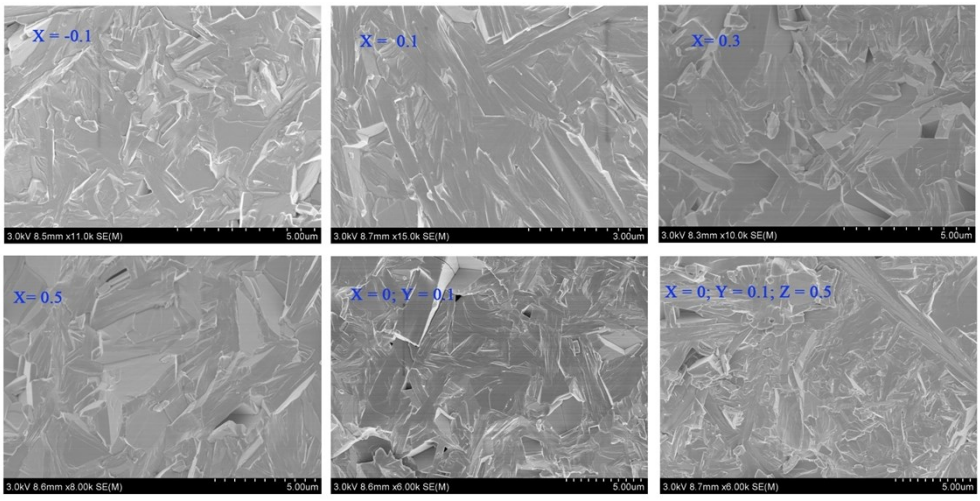

Figure S11 *SEM micrographs for the cross-sections of the $Bi_{11}Fe_{3+x}Ti_{6-x}O_{33}$ and $La_zBi_{11-z}Fe_{3-y}Co_yTi_6O_{33}$ ceramics. All the samples are densely packed with plate-like crystalline grains, which is typical of the Aurivillius bismuth layered compounds because of the preferential growth of the a-b plane. The low-level substitution seems have no apparent impact on the morphology. Therefore, we believe that the shift of the position, width and intensity of XRD peaks is intrinsic to the atomic structure of the samples. Meanwhile, we also believe that the observed ferroelectric property should be correlated with the intrinsic crystal structures.*

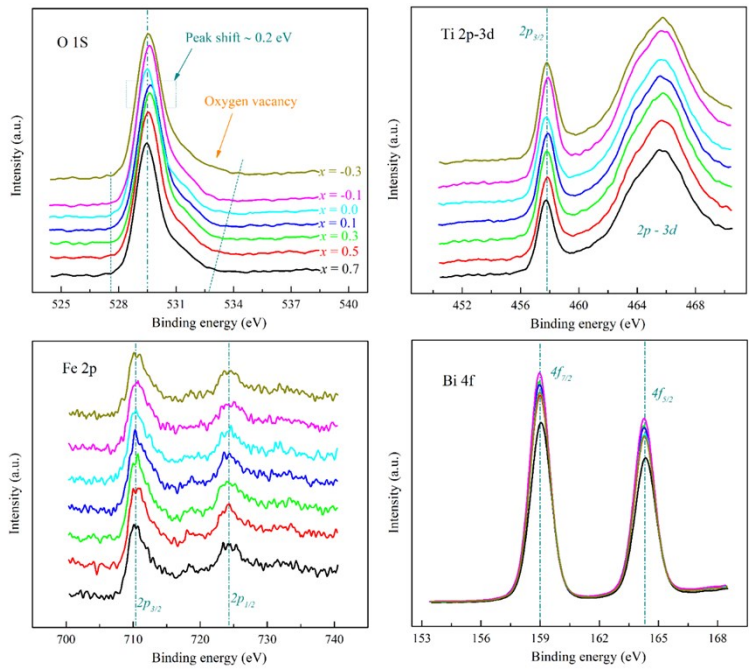

Figure S12. *The XPS spectra of (a) O 1s, (b) Ti 2p-3d (c) Fe 2p and (d) Bi 4f of* $Bi_{11}Fe_{3+x}Ti_{6-x}O_{33}$. *All the XPS spectra were adjusted according to C 1s at 284.6 eV. The results indicate that the change of the Fe/Ti ratio does not cause valence change of Fe, Ti and Bi, but directly affect the oxygen vacancy. The slight shift of the O1s peak in the mixed-layer samples might suggest the larger structural distortions.*

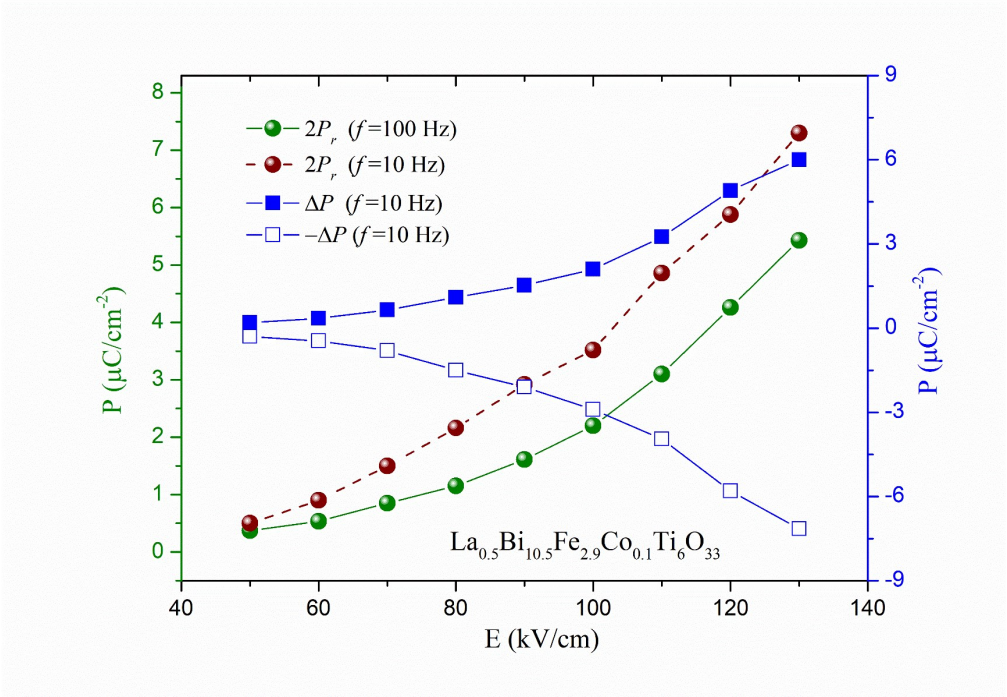

Figure S13. *ΔP from PUND measurement and* $2P_r$ *from the P-E loops of* $La_{0.5}Bi_{10.5}Fe_{2.9}Co_{0.1}Ti_6O_{33}$ *at RT under different applied electric fields and measured frequencies.*

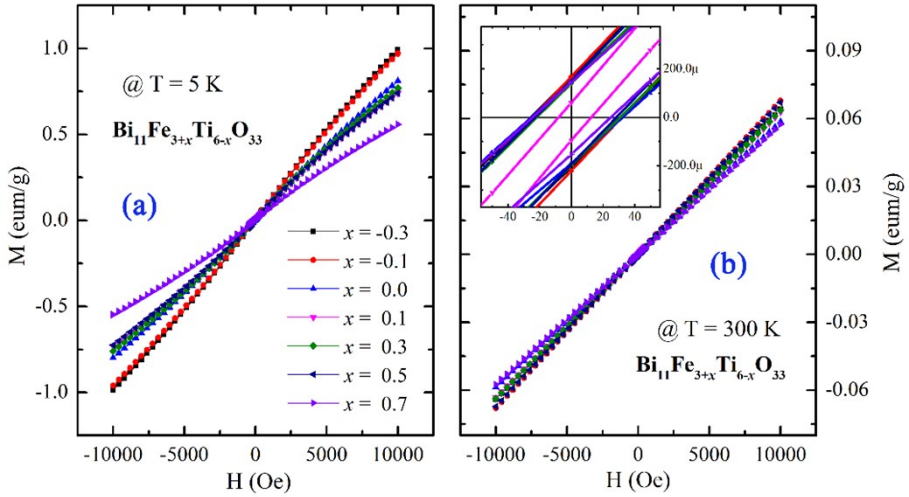

Figure S14. *The M-H loops for the $Bi_{11}Fe_{3+x}Ti_{6-x}O_{33}$ at (a) 5 K and (b) 300 K.*

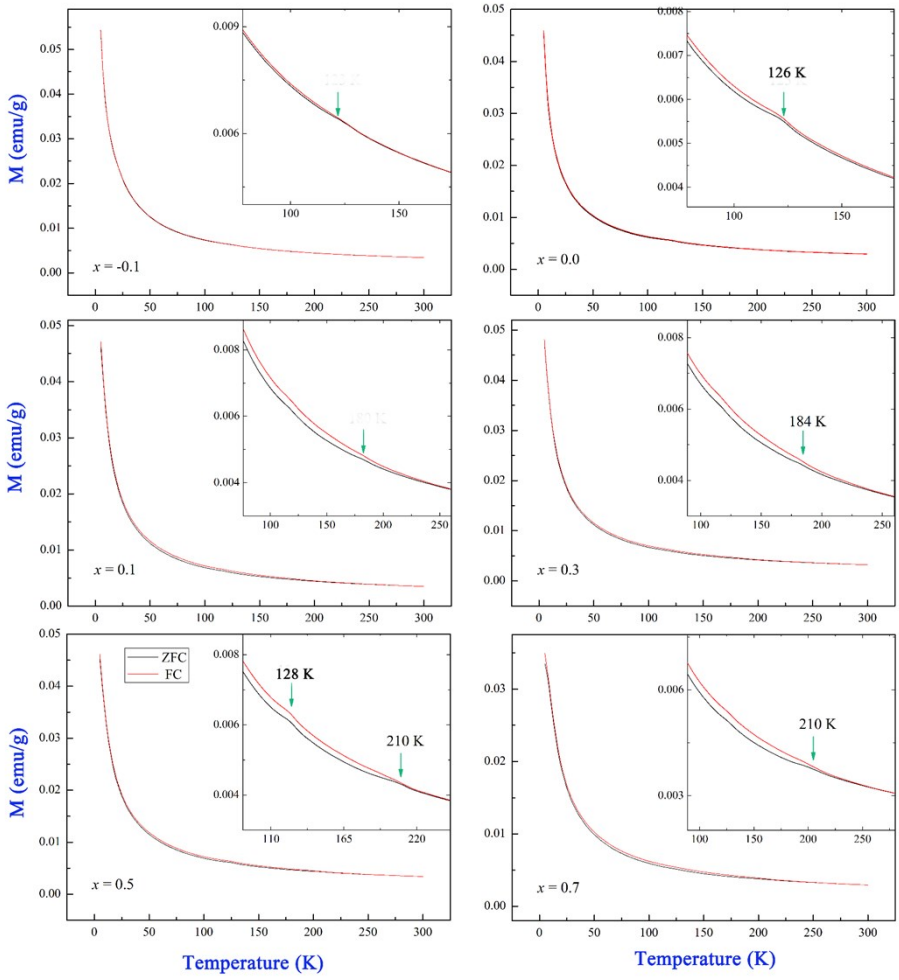

Figure S15. *The ZFC-FC curves for the $Bi_{11}Fe_{3+x}Ti_{6-x}O_{33}$ at 10~300 K.*

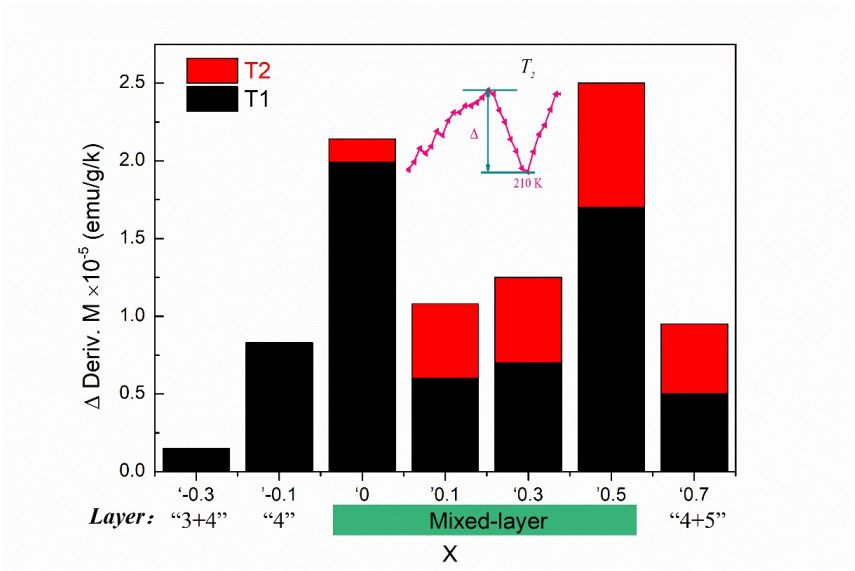

Figure S16. *The correlation between the corresponding peak intensity of T1 and T2 from the Figure 6b and the layer-structure of the samples. The inset is the estimated Δ of the T2 for x = 0.5 as an example.*

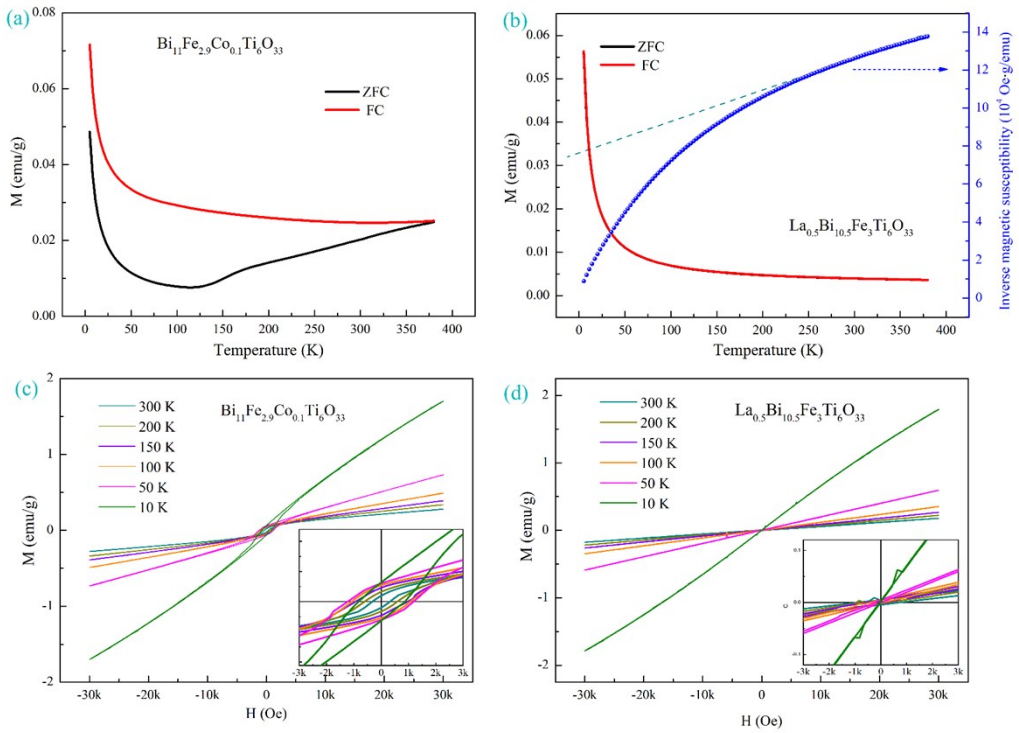

Figure S17. *The ZFC-FC curves under 500 Oe and the M-H loops at different temperatures for the chosen (a,c) $Bi_{11}Fe_{2.9}Co_{0.1}Ti_6O_{33}$ and (b,d) $La_{0.5}Bi_{10.5}Fe_3Ti_6O_{33}$.*

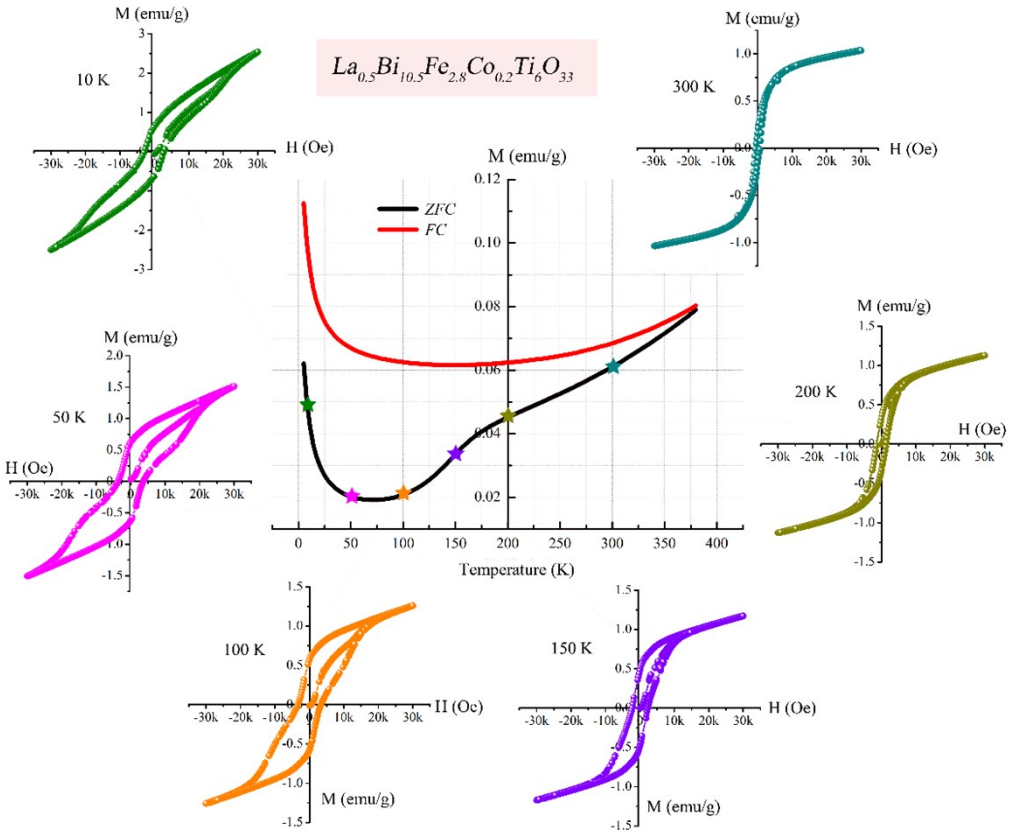

Figure S18. *Magnetic hysteresis loops and the ZFC-FC curves measured under 500 Oe for* $La_{0.5}Bi_{10.5}Fe_{2.8}Co_{0.2}Ti_6O_{33}$.

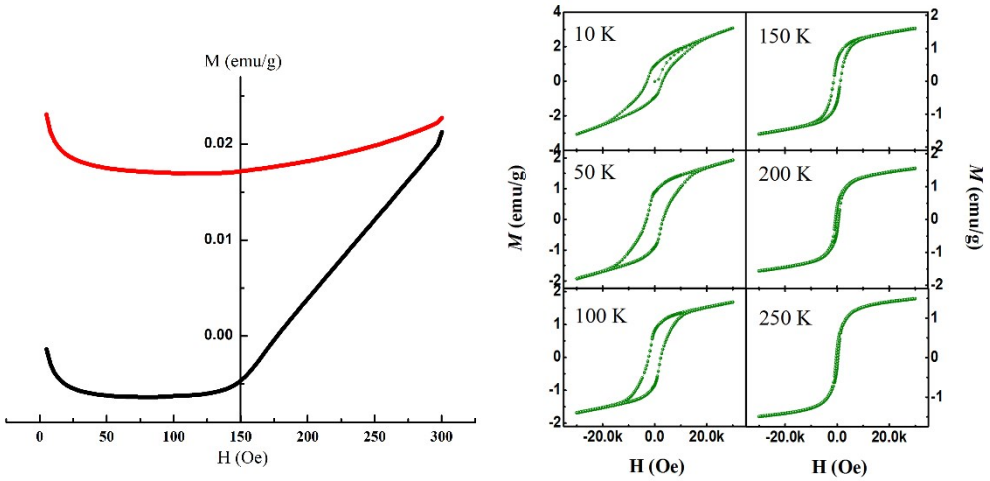

Figure S19. *The ZFC-FC curves measured under 100 Oe and magnetic hysteresis loops at different temperatures for the* $Bi_{11}Fe_{2.7}Co_{0.3}Ti_6O_{33}$.

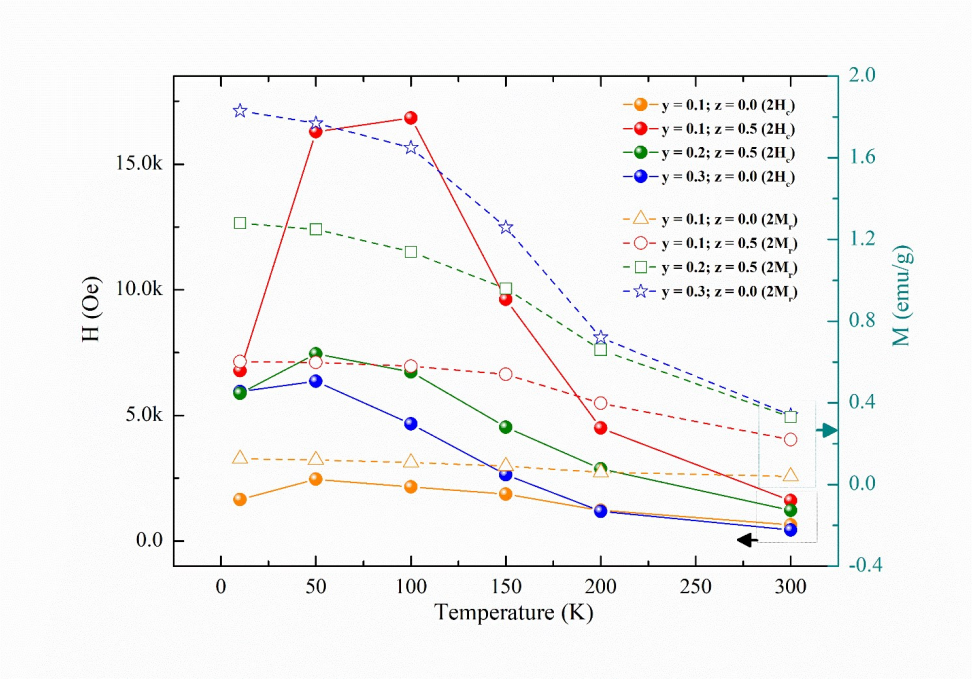

Figure S20. *The temperature dependence of remnant magnetization ($2M_r$) and magnetic coercive fields ($2H_c$) for $La_zBi_{11-z}Fe_{3-y}Co_yTi_6O_{33}$ ($y=0.1$ and $z=0.0$; $y = 0.1$ and $z= 0.5$; $y = 0.2$ and $z =0.5$; $y=0.3$ and $z = 0.0$).*

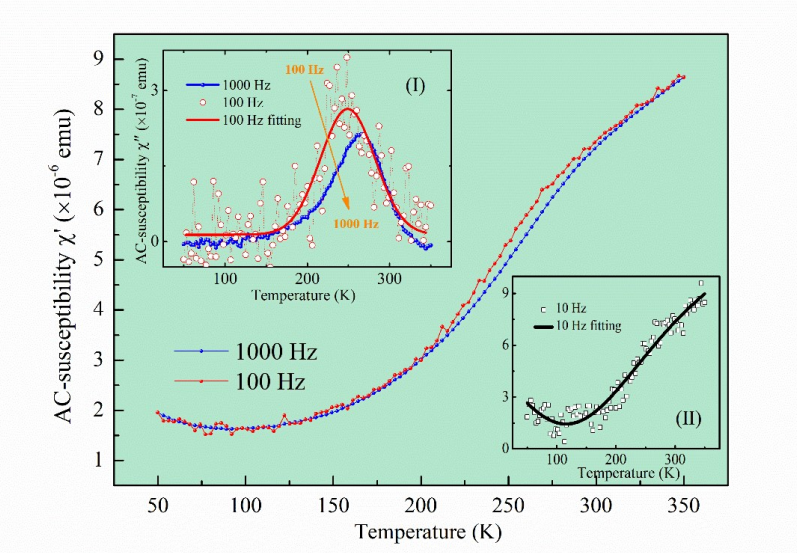

Figure S21. *AC susceptibility (real χ′) of the $Bi_{11}Fe_{2.9}Co_{0.1}Ti_6O_{33}$ sample in the temperature interval of 50-350 K at 100 and 1000 Hz. The inset (Ⅰ) is imaginary components (χ″) of the susceptibility at 100 and 1000 Hz. The inset (Ⅱ) is real components (χ′) of the susceptibility at 10 Hz. χ″ exhibits a pronounced peak indicating the presence of a relaxation process. With increasing the frequency, the maximum of χ″ shifts to higher temperature, which is characteristic of spin glass.*

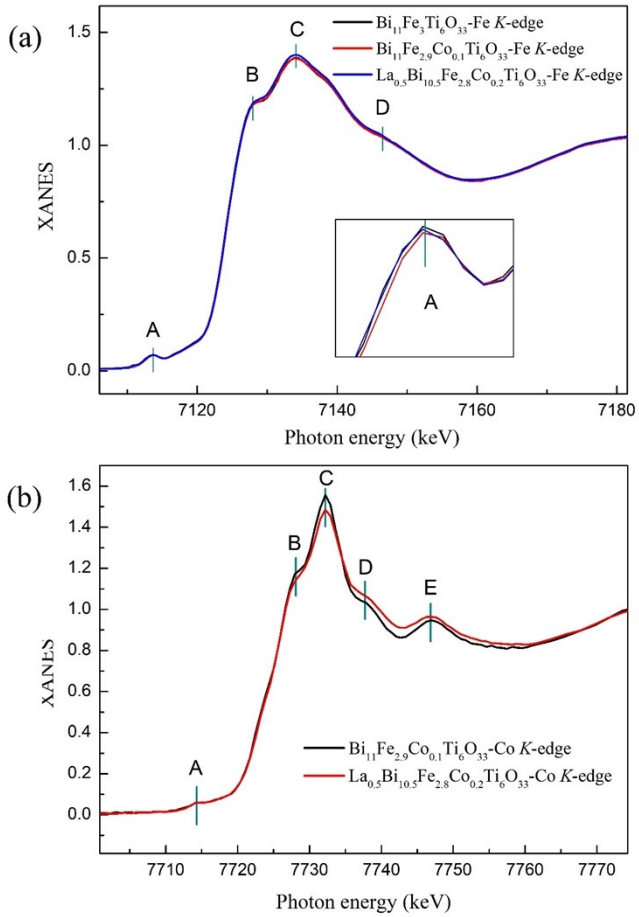

Figure S22. *(a) XANES Fe K-edge spectra of the $Bi_{11}Fe_3Ti_6O_{33}$, $Bi_{11}Fe_{2.9}Co_{0.1}Ti_6O_{33}$ and $La_{0.5}Bi_{10.5}Fe_{2.8}Co_{0.2}Ti_6O_{33}$ samples. (b) XANES Co K-edge spectra of the $Bi_{11}Fe_{2.9}Co_{0.1}Ti_6O_{33}$ and $La_{0.5}Bi_{10.5}Fe_{2.8}Co_{0.2}Ti_6O_{33}$ samples.*

Table S1 *Comparison of electrical and magnetic properties of $BiFeO_3$ ceramics reported recently and the samples in this work.*

Material system	***Phase structure***	***2Pr ($\mu C/cm^2$)***	***2E_c (kV/cm)***	***Mr (emu/g)***	***Ref.***
$BiFeO_3$	*R*	*10*	*70*	*—*	*"Multiferroic bismuth ferrite-based materials for multifunctional applications: Ceramic bulks, thin films and nanostructures", Progress in Materials Science 2016, 84, 335–402.*
$Bi_{0.9}La_{0.1}FeO_3$	*R*	*6*	*—*	*—*	
$Bi_{0.85}La_{0.15}FeO_3$	*Ps + triclinic*	*12*	*60*	*0.074*	
$Bi_{1-x}La_xFeO_3$	*R-triclinic-p-T*	*9.8*	*—*	*0.2*	
$BiFe_{0.95}Co_{0.05}O_3$	*R*	*—*	*—*	*0.7*	
$BiFe_{0.95}Ho_{0.05}O_3$	*R*	*8.4*	*75*	*0.026*	
$Bi_{0.85}La_{0.15}Fe_{0.9}Ti_{0.1}O_3$	*R-T*	*—*	*—*	*0.25*	
$Bi_{0.9}La_{0.1}Fe_{0.97}Co_{0.03}O_3$	*—*	*—*	*—*	*0.23*	
$Bi_{11}Fe_{3.3}Ti_{5.7}O_{33}$	*O*	*5.3 (100Hz)*	*84*	*1.6×10^{-4}*	*This work*
$La_{0.5}Bi_{10.5}Fe_{2.9}Co_{0.1}Ti_6O_{33}$	*O*	*~6.9 (100Hz) ~9.1 (10Hz)*	*~89 (100HZ) ~100 (10HZ)*	*0.12 (300K) 0.29 (50K)*	*This work*